J Mol Model (2013) 19:1039–1047
DOI 10.1007/s00894-012-1649-z

ORIGINAL PAPER

Insight into the dynamic interaction between different flavonoids and bovine serum albumin using molecular dynamics simulations and free energy calculations

Xiaodi Niu · Xiaohan Gao · Hongsu Wang · Xin Wang · Song Wang

Received: 23 March 2012 / Accepted: 14 October 2012 / Published online: 1 November 2012

Abstract In this study, the binding of Bovine serum albumin (BSA) with three flavonoids, kaempferol-3-*O*-a-L-rhamnopyranosyl-(1–3)-a-L-rhamnopyranosyl-(1–6)-b-D-galacto- pyranoside (drug 1),kaempfol-7-*O*-rhamnosyl-3-*O*-rutinoside (drug 2)andkaempferide-7-O-(4”-*O*-acetylrhamnosyl)-3-*O*-ruti- noside (drug 3) is investigated by molecular docking, molecular dynamics (MD) simulation, and binding free energy calculation. The free energies are consistent with available experimental results and suggest that the binding site of BSA-drug1 is more stable than those of BSA-drug2 and BSA-drug3. The energy decomposition analysis is performed and reveals that the electrostatic interactions play an important role in the stabilization of the binding site of BSA-drug1 while the van der Waals interactions contribute largely to stabilization of the binding site of BSA-drug2 and BSA-drug3. The key residues stabilizing the binding sites of BSA-drug1, BSA-drug2 and BSA-drug3 are identified based on the residue decomposition analysis.

Keywords Binding energy · Bovine serum albumin · Flavonoid · Molecular dynamics (MD) simulation

X. Niu · X. Gao · H. Wang · X. Wang · S. Wang (✉)
Department of Food quality and Safety, Jilin University, Changchun 130062, People’s Republic of China
e-mail: ws@jlu.edu.cn

X. Niu
e-mail: niuxd@jlu.edu.cn

X. Niu · S. Wang
State Key Laboratory of Theoretical and Computational Chemistry, Institute of Theoretical Chemistry, Jilin University, Changchun 130061, People’s Republic of China

Introduction

Many flavonoids are found in nature, and it has been reported that these natural products have various biological properties, for example, anti-oxidative [1, 2], anti-mutagenic activities [3–5], anti-inflammatory activity [6], antifungal activity [7] and antitumor activity [8]. Therefore, flavonoids have been linked with many health benefits, and foods rich in flavonoids have attracted most interest in recent years. Most flavonoids consist of a benzene ring (A-ring) condensed with a six-membered ring (C-ring) which carries a phenyl group (B-ring) as a substituent in the 2-position. Recent studies have shown that these biological activities vary with the number and substitution positions of hydroxyl and/or methoxy groups in the flavonoid molecules [9–11]. The structural difference of flavonoids also affects their binding process to serum albumin significantly [12, 13].

Serum albumin is the major soluble protein in the circulatory system, which has many physiological functions, such as maintaining the osmotic pressure and pH of blood and as carriers transporting a great number of endogenous and exogenous compounds such as fatty acids, amino acids, drugs and pharmaceutical [14]. The drug-serum albumin interaction plays a dominant role in drug disposition and efficacy. Bovine serum albumin (BSA) is usually employed as a model protein because of its low cost, availability and structural similarity with human serum albumin (HSA) [15, 16].

In recent research, most works have reported the binding process between flavonoids and bovine serum albumin, using parameters such as binding constant, binding affinity, binding distance, and energy transfer by means of various spectroscopic methods [17–19]. For example, the three

flavonoids including naringenin, hesperetin and apigenin binding to bovine serum albumin (BSA) at pH 7.4 was studied by fluorescence quenching, synchronous fluorescence and UV–vis absorption [20]. Yuping Zhang et. al. [21] reported that four flavonids quercetin, luteolin, taxifolin and (+)-catechin with the same A- and B- rings but different C-ring substitutents had been investigated for their binding to bovine serum albumin (BSA) in the absence and presence of Cu^{2+} using fluorescence, UV-visible and circular dichroism. Xiaolei Shi co-worker [22] pointed out that three kinds of flavonoids have strong ability to quench the intrinsic fluorescence of BSA by forming complexes. The binding constants, number of binding sites, thermodynamic parameters and energy transfer were also obtained. However, the mechanisms about how the drugs bind to BSA at atomic level are not clear, which could provide useful information to further assist in drug design. This makes the study on the dynamic characteristics more significant. As a benzene ring condensed with a six-membered ring which carries a phenyl group is a key part of many flavonoids for their potency and activation, three flavonoids, kaempferol-3-O-a-L-rhamnopyranosyl-(1–3)-a-L-rhamnopyranosyl-(1–6)-b-D-galacto- pyranoside (drug 1), kaempfol-7-O-rhamnosyl-3-O-rutinoside (drug 2)andkaempferide-7-O-(4”-O-acetylrhamnosyl)-3-O-ruti- noside (drug 3), are selected in this study and their chemical structures are shown in Fig. 1. Accordingly, based on the result from the homology modeling and molecular docking, molecular dynamics (MD) simulations, calculation of binding free energy, and ligand-residue interaction decomposition were performed.

Materials and methods

Homology modeling of BSA

Sequence alignment was done with the on-line BLAST (http://www.ncbi.nlm.nih.gov) [23]. The 3D structure of BSA was built with the on-line version of 3D-JIGSAW [24, 25] and was subjected to further 50 ns molecular dynamics using Gromacs 4.5.2 software package [26].

The geometries of drug1, drug2, and drug3 were optimized at the B3LYP/6-31G* level using the Gaussian 03 program [27].

Molecular docking calculation

The initial structure of BSA was obtained from the homology modeling. To obtain the starting structure of the drugs-BSA complex for molecular dynamics (MD) simulation, a standard docking procedure for a rigid protein and a flexible ligand was performed with AutoDock 4 [28, 29]. The Lamarckian genetic algorithm (LGA) was applied in the docking calculations. All of the torsional bonds of the drugs were free to rotate while BSA was held rigid. Then, the polar hydrogen atoms were added for BSA using the AutoDock tools, and Kollman united atom partial charges [30] were assigned. A total of 150 independent runs were carried out with a maximum of energy evaluations to 25,000,000 and a population size to 300. A grid box (70×70×70) with spacing of 1.000 Å was created and centered on the mass center of the ligand. Energy grid maps for all possible ligand atom types were generated using Autogrid 4 before performing the docking.

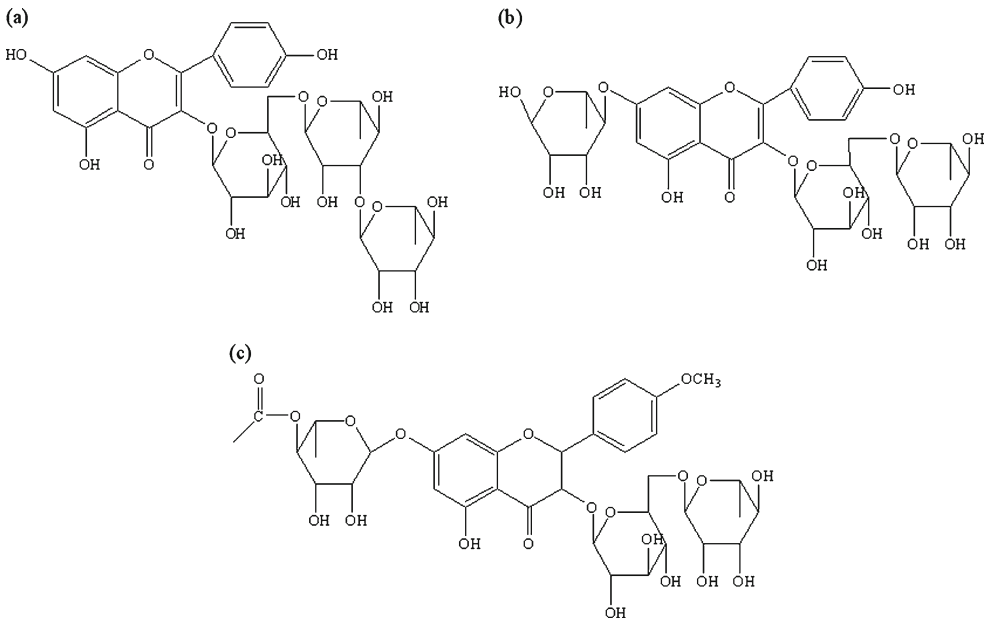

Fig. 1 Structures of drug1 (**a**), drug2 (**b**), and drug3 (**c**)

The clusters were ranked according to the lowest energy representative in each cluster. The lowest energy conformation in the most populated cluster was chosen for further study [31].

Molecular dynamics simulations

All of the simulations and the analysis of the trajectories were performed with Gromacs 4.5.2 software package [26] using the Charmm27 force field and the TIP3P water model [32]. The BSA-drug systems were first energy relaxed with 2000 steps of steepest-descent energy minimization followed by another 2000 steps of conjugate-gradient energy minimization. The systems were then equilibrated by a 500 ps of MD run with position restraints on the protein and ligand to allow for relaxation of the solvent molecules. The first equilibration run was followed by a 25 ns MD run without position restraints on the solute. The first 20 ns of the trajectory were not used in the subsequent analysis to minimize convergence artifacts. The equilibration of the trajectory was checked by monitoring the equilibration of quantities, such as the root-mean-square deviation (rmsd) with respect to the initial structure, the internal protein energy, and fluctuations calculated for different time intervals. The electrostatic term was described with the particle mesh Ewald algorithm. The LINCS [33] algorithm was used to constrain all bond lengths. For the water molecules, the SETTLE algorithm [33] was used. A dielectric permittivity, $\varepsilon=1$, and a time step of 2 fs were used. All atoms were given an initial velocity obtained from a Maxwellian distribution at the desired initial temperature of 300 K. The density of the system was adjusted during the first equilibration runs at *NPT* condition by weak coupling to a bath of constant pressure ($P_0=1$ bar, coupling time $\tau_P=0.5$ ps) [34]. In all simulations, the temperature was maintained close to the intended values by weak coupling to an external temperature bath with a coupling constant of 0.1 ps. The proteins and the rest of the system were coupled separately to the temperature bath. The structural cluster analysis was carried out using the method described by Daura and co-workers with a cutoff of 0.25 nm [34].

The parameters of drug1, drug2, and drug3 were estimated with the antechamber programs [35] and the structures were shown in Fig. 1. AM1-BCC partial atomic charges from the Amber suite of programs [36].

Analysis of the trajectories was performed using VMD, PyMOL analysis tools and Gromacs analysis tools.

Calculation of binding free energy

In this work, the binding free energies are calculated using molecular mechanics/Poisson-Boltzman surface area (MM-PBSA) approach [37–40] supplied with Amber 10 package. We choose a total number of 100 snapshots evenly from the last 10 ns on the MD trajectory with an interval of 10 ps. The MM-PBSA method can be conceptually summarized as:

$$\Delta G_{bind} = \Delta G_{complex} - \left[\Delta \mathrm{G}_{\mathrm{protein}} + \Delta \mathrm{G}_{\mathrm{lig}}\right] \quad (1)$$

$$\Delta G_{bind} = \Delta H - \mathrm{T}\Delta \mathrm{S}, \quad (2)$$

where ΔH of the system is composed of the enthalpy changes in the gas phase upon complex formation (ΔE_{MM}) and the solvated free energy contribution (ΔG_{sol}), while $-T\Delta S$ refers to the entropy contribution to the binding. Equation (2) can then be approximated as shown in Eq. (3):

$$\Delta G_{bind} = \Delta E_{MM} + \Delta G_{sol} - \mathrm{T}\Delta \mathrm{S}, \quad (3)$$

where ΔE_{MM} is the summation of the van der Waals (ΔE_{vdw}) and the electrostatic (ΔE_{ele}) interaction energies.

$$\Delta E_{MM} = \Delta E_{vdw} + \Delta E_{ele}. \quad (4)$$

In addition, ΔG_{sol}, which denotes the solvation free energy, can be computed as the summation of an electrostatic component ($\Delta G_{ele,sol}$) and a nonpolar component ($\Delta G_{nonpolar,sol}$), as shown in Eq. (5):

$$\Delta G_{sol} = \Delta G_{ele,sol} + \Delta G_{nonpolar,sol}. \quad (5)$$

Ligand-residue interaction decomposition

The interactions between drugs and each residue in the binding site of α-HL are analyzed using the MM-GBSA decomposition process applied in the MM-GBSA module in Amber 10. The binding interaction of each ligand-residue pair includes three terms: the Van der Waals contribution (ΔE_{vdw}), the electrostatic contribution (ΔE_{ele}), and the solvation contribution (ΔE_{sol}). All energy components are calculated using the same snapshots as the free energy calculation.

Results and discussion

Determination of the binding mode of BSA with drug1, drug2, and drug3

Because flavonoids binds to the BSA, we were interested in identifying the potential binding of drugs to BSA in the active site via molecular docking and molecular dynamics simulation using AutoDock 4.0 and Gromacs 4.5.1 software package. The initial structure of the monomeric BSA was obtained from homology modeling, as previously reported [41].

To explore the mechanism of BSA bound with drug1, drug2 and drug3, we determined the preferential binding

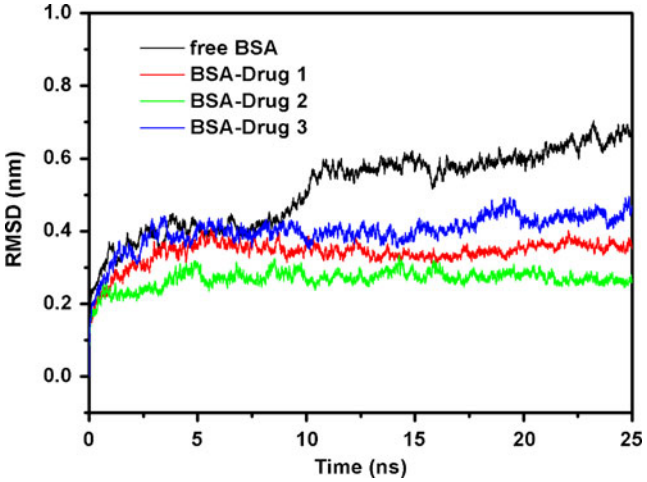

Fig. 2 The root-mean-square deviations (RMSD) of all the atoms of BSA-drugs complexes with respect to their initial structures as function of time

mode of BSA with drugs by 25-ns molecular dynamics simulations based on the docking results. Initially, the root-mean-square deviations (RMSD) of backbone C_α atoms are analyzed to examine whether each system reaches equilibrium and it can be seen that the complex was found to reach equilibrium at 10 ns, as is shown in Fig. 2. The drug1, drug2, and drug3 are bound to BSA and the best solutions are given in Fig. 3. It is clear that three drugs can bind to BSA via hydrogen bonding and hydrophobic interactions. Over the time course of the simulation, drugs localize to the catalytic pocket (50 to 200, 400 to 600).

The predicted binding mode of drug1 with BSA is illustrated in Fig. 3, and the electrostatic potentials of the residues around the binding site are mapped using APBS software, [42] as shown in Fig. 3. In detail, the binding model of drug1 with the BSA (Fig. 4a) revealed that the hydroxyl group and oxygen of drug1 both formed hydrogen bonds with the side chains amino and carbonyl of Gln 57, carbonyl of Asp 135, and amino group of Lys 138. As is shown in Fig. 4b, the number of hydrogen bonds fluctuates between 4 and 6 within the simulation time, which indicates that there are always 4–6 hydrogen bonds between drug1 and BSA. Moreover, the electropositive side chains of Lys138 and Gln57 form electrostatic interactions with drug1. It can be seen that Gln57 anchor the benzene ring of drug1, and Lys138 plays an important role in stabilizing the 4H-chromen-4-one moiety of drug1, which will be confirmed by energy decomposition analysis. In addition, the binding modes of drug2 and drug1 are similar, as is shown in Fig. 4c. The hydroxyl groups of drug2 can form hydrogen bonds with the side chain carbonyl of Glu164 and Asp535

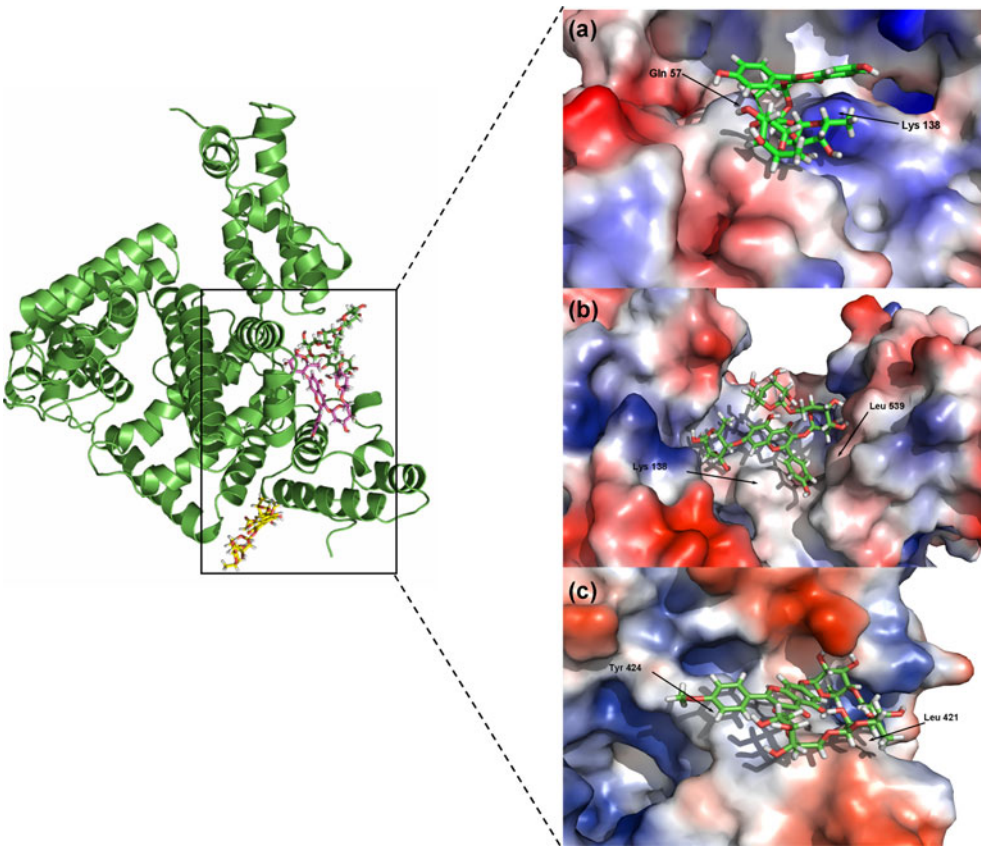

Fig. 3 The predicted binding mode of drugs (*green*) (**a** drug1; **b** drug2; **c** drug3) in the BSA binding pocket obtained from MD simulation

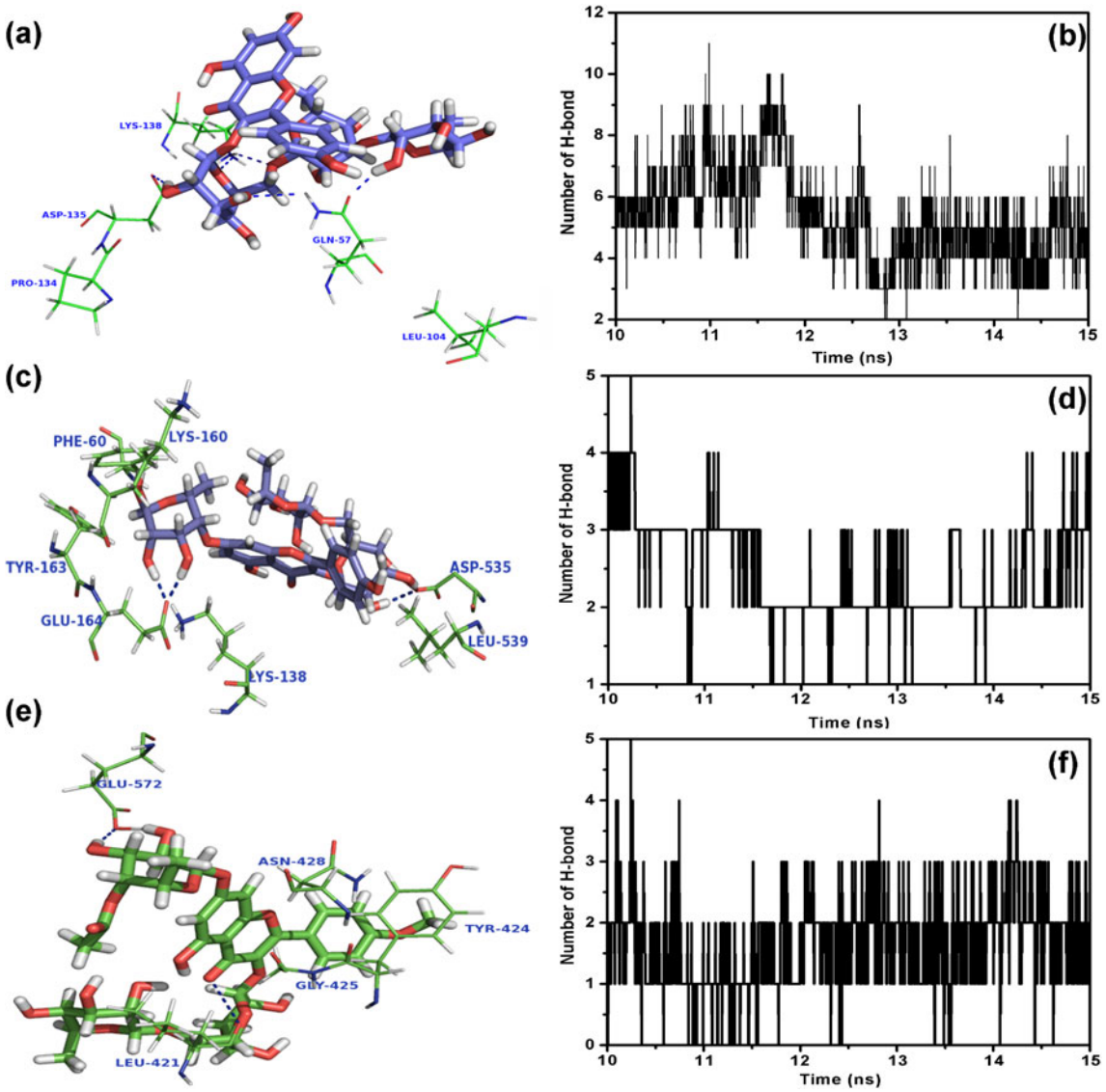

Fig. 4 Predicted binding modes of BSA with the drug1 (**a**), drug2 (**c**), and drug3 (**e**) are shown with labels for key residues. The number of hydrogen bonds between drug1 (**b**), drug2 (**d**), drug3 (**f**) and BSA during the last 10-ns simulation is shown

and the benzene ring can form hydrophobic interactions with Lys138 and Leu539. As is shown in Fig. 4d, the number of hydrogen bonds fluctuates between 2 and 4 within the simulation time, which indicates that there are always 2–4 hydrogen bonds between drug2 and BSA. However, the position of drug3 is on the other side of the pocket. Figure 4e show that in the BSA-drug3 complex, the benzene ring of drug3 is parallel with the benzene ring plane of residue Tyr424, and Tyr424 is close to drug3. In this case, a π-π interaction between the two conjugate systems probably exists, leading to a strong interaction between the residue and drug3. In addition, there are two hydrogen bonds between drug3 and Leu421 and Glu572. The number of hydrogen bonds fluctuates between 1 and 3 within the simulation time, which indicates that there are always 1–3 hydrogen bonds between drug3 and BSA, as is shown in Fig. 4f. The corresponding results of H-bonds between BSA and drugs were shown in Table 1.

The root mean square fluctuation (RMSF) of the residues around the drugs binding sites of BSA in the BSA-drugs complexes and in free BSA were calculated to reveal the flexibility of these residues. The RMSF of these residues are shown in Fig. 5, clearly depicting different flexibilities in the binding sites of BSA in the presence and absence of drugs. In Fig. 5a and b, the residues (50–200) in the BSA binding site that bind with drug1 and drug2 show a small degree of flexibility with RMSF of less than 5.00 Å when compared with free BSA, indicating that these residues seem to be more rigid as a result of binding to drug1 and drug2. In Fig. 5c, the residues (400–600) in the BSA

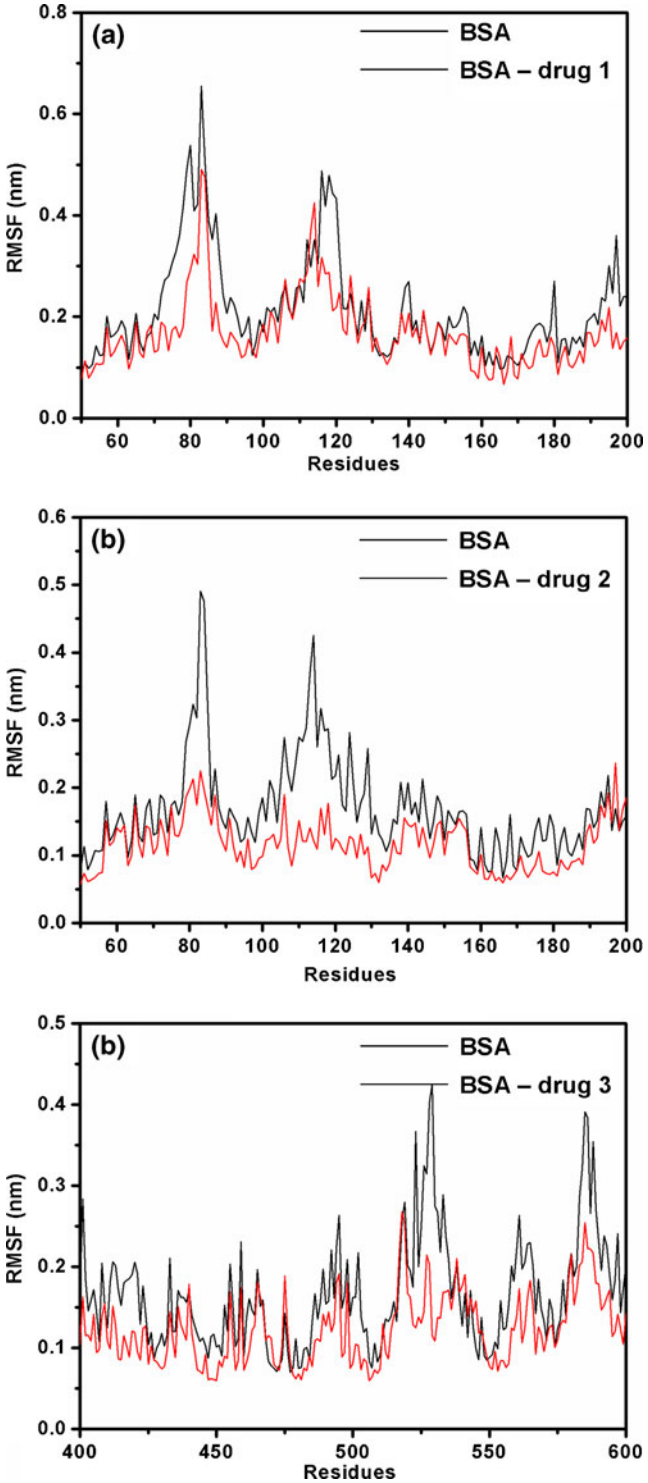

Fig. 5 RMSF of residues around the ligand-binding site of BSA (50–200, 400–600) in the BSA-drugs complexes (**a** drug1; **b** drug2; **c** drug3) and free BSA during the last 10-ns simulation time

binding site that bind with drug3 also show a small degree of flexibility with RMSF of less than 2.5 Å when compared with free BSA.

Identification of the binding sites in the BSA-drugs complexes

To gain more information about the residues surrounding the binding site and their contribution to the whole system, the electrostatic, Van der Waals, solvation and total contribution of the residues to the binding free energy of BSA-drugs were calculated with the molecular mechanics generalized Born surface area (MM-GBSA) method [43, 44]. The calculation was performed over the 50 MD snapshots taken from the last 20-ns simulation. The summations of the per residue interaction free energies were separated into Van der Waals (ΔE_{vdw}), electrostatic (ΔE_{ele}), solvation (ΔE_{sol}), and total contribution (ΔE_{total}). The energy contributions from the selected residues are summarized in Fig. 6a, b and c.

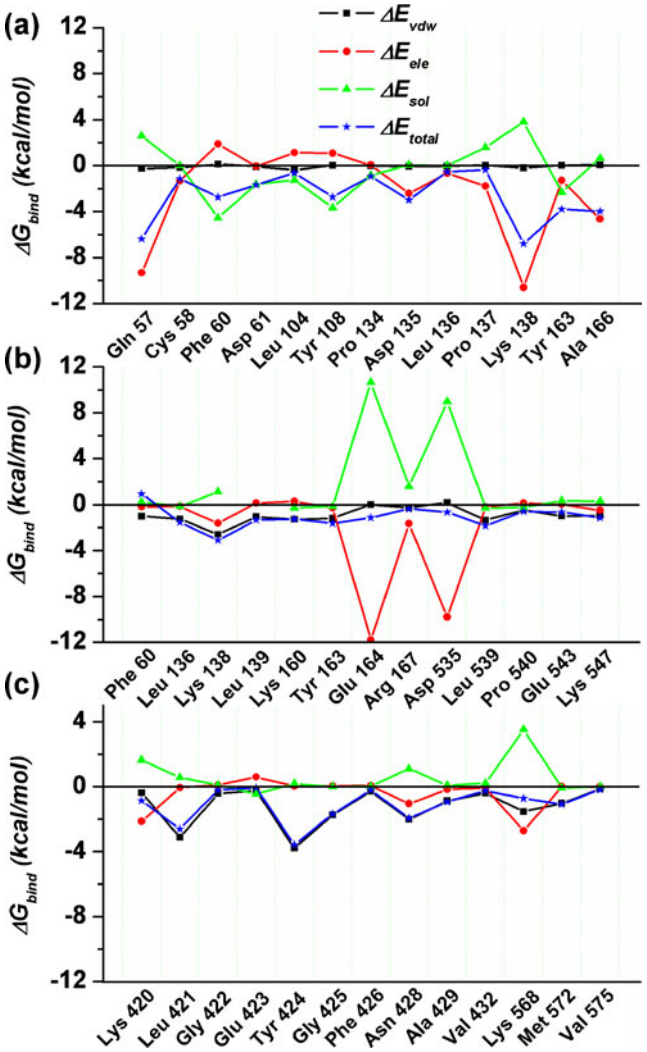

Fig. 6 Decomposition of the binding energy on a per-residue basis in the BSA-drug1 complex (**a**), BSA-drug2 complex (**b**) and BSA-drug3 complex (**c**)

Table 1 BSA-drugs H-bonds from MD simulations

Acceptor	Donor	Presence %	Distance (Å)
Drug1:			
lig > O	Lys138 N-H	95.2	2.2±0.12
lig > O		93.6	1.9±0.15
lig H-O	Gln57 N-H	91.5	2.5±0.11
Gln57 C=O	lig O-H	93.4	1.7±0.16
Asp135 C=O	lig O-H	67.4	1.9±0.20
Drug2:			
Glu164 C=O	lig O-H	89.5	1.7±0.13
	lig O-H	88.7	1.5±0.15
Asp535 C=O	lig O-H	69.7	2.0±0.19
Drug3:			
Leu421 C=O	lig O-H	47.1	3.3±0.23
Glu572 C=O	lig O-H	84.2	2.0±0.19

As shown, in the BSA-drug1 complex, Lys138 has an appreciable electrostatic (ΔE_{ele}) contribution, with a ΔE_{ele} of ≤ −10 kcal mol^{-1} (Fig. 6a). In fact, Lys138 is close to the glycosides moiety of drug1, and two electrostatic interactions exist, leading to two strong H-bonds between BSA and drug1. In addition, residue Gln57, with a ΔE_{ele} of ≤ −9 kcal mol^{-1}, has another strong electrostatic interaction with the ligand because of the close proximity between the carbonyl of residue Gln57 and glycosides moiety of drug1, which promotes two strong H-bonds in the complex. Except for the residues Phe60 and Tyr108, the majority of the decomposed energy interaction originated from electrostatic interactions, apparently through hydrophilic interactions, while the Van der Waals contribution appeared to be a minor influence on those key residues in BSA-drug1 complex formation. However, for BSA-drug2 complex, except for the residues Glu164 and Asp535, the majority of the decomposed energy interaction originated from Van der Waals interactions. Lys138 has the strongest attraction interaction (with van der Waals term of −2.3 kcal mol^{-1}). Glu164 and Asp535 have two large electrostatic (−12 kcal mol^{-1} and −10 kcal mol^{-1}) terms, while solvation (ΔE_{sol}) shows unfavorable contributions at 11 kcal mol^{-1} and 9 kcal mol^{-1}, which results in that the total energy contributions of Glu164 and Asp535 are weak. Similarly, for BSA-drug3 complex, the van der Walls interactions of Leu421 and Tyr424 are −3.0 kcal mol^{-1} and −4.0 kcal mol^{-1}, respectively, which suggests that both are key residues near the electropositive groups of drug3 as observed from binding modes (Fig. 6b and c).

Binding affinity of BSA-drugs

In addition, the total binding free energy for the BSA-drug complexes and their detailed energy contributions calculated according to the MM-PBSA approach, are summarized in Table 2. The ΔG_{bind} can be divided into polar ($\Delta G_{ele,sol}$ + ΔE_{ele}) and nonpolar energies ($\Delta G_{nonpolar}$ + ΔE_{vdw}). The free energy of drug1 binding to BSA is primarily derived from the $\Delta G_{ele,sol}$ + ΔE_{ele} at −52.07 kcal mol^{-1}, while the $\Delta G_{nonpolar}$ + ΔE_{vdw} shows a likely unfavorable contribution at 29.29 kcal mol^{-1}. This is due to the intermolecular electrostatic energy, which is mainly achieved from the drug1-binding residues. With the summation of the solute entropy term (~10.7 kcal mol^{-1}), an estimated ΔG_{bind} of −12.08 kcal mol^{-1} was found for drug1, suggesting that drug1 can bind to and interact with the binding site of BSA through electrostatic energy, while for drug2 and drug3, the free energies are primarily derived from the nonpolar energies ($\Delta G_{nonpolar}$ + ΔE_{vdw}) at −10.34 kcal

Table 2 Calculated energy components, binding free energy (kcal mol^{-1}) of three flavonoids binding to active site of BSA. K_A is the binding constant, reflecting the reaction degree of BSA and flavonoids and n is the number of binding sites

Energy components (kcal mol^{-1})	Drug 1	Drug 2	Drug 3
ΔE_{ele}	−47.51±6.96	−2.72±3.87	−2.97±7.60
ΔE_{vdw}	−34.58±2.98	−39.23±7.38	−43.85±3.43
ΔE_{MM}	−82.09±7.87	−41.95±9.45	−46.82±9.82
$\Delta G_{ele,sol}$	−4.56±0.22	−3.89±0.26	−1.68±0.20
$\Delta G_{nonpolar,sol}$	63.87±6.46	28.89±8.15	30.30±9.14
ΔG_{sol}	59.31±6.35	25.00±8.15	28.62±4.27
$\Delta G_{ele,sol}$ + ΔE_{ele}	−52.07±7.18	−6.61±7.47	−4.64±7.97
$\Delta G_{nonpolar}$ + ΔE_{vdw}	29.29±4.71	−10.34±5.61	−13.55±4.71
ΔG_{total}	−22.78±2.83	−16.95±2.99	−18.19±2.51
$-T\Delta S$	10.7±2.51	9.87±2.01	9.19±2.47
ΔG_{bind}	−12.08±1.23	−7.08±1.48	−9.00±1.52
K_A (1×10^4) L·mol^{-1} [22]	0.89	0.30	0.41
n [22]	0.92	0.81	0.83
r [22]	0.9998	0.9778	0.9971

mol^{-1} and −13.55 kcal mol^{-1}, respectively. The $\Delta G_{ele,sol}$ + ΔE_{ele} show a minior contribution at −6.61, −4.64 kcal mol^{-1}, respectively, which suggests that drug2 and drug3 can bind to BSA through van der Waals energy.

Moreover, the MM-GBSA calculation predicted that drug2 and drug3 bound more weakly to BSA than did drug1 (−7.08 kcal mol^{-1} for drug2 and −9.00 kcal mol^{-1} for drug3), as shown in Table 2. The calculations for drug2 and drug3 revealed that these two drugs resulted in a decrease of approximately 3 to 5 kcal mol^{-1} of binding energy compared to drug1. According to the experimental results [22], the binding constants, K_A of the interaction between drugs and BSA decrease in the following order: drug1 > drug3 > drug2, which means that drug1 has the strongest ability to bind to BSA and drug2 has the weakest ability, as shown in Table 2. The calculated binding free energies are in good agreement with the experimental data. We believe that the MD simulations generated the reliable BSA-drugs complexes.

Conclusions

In summary, the current computational study insights into the structure and interactions for the binding of three flavonoids to BSA at the atomic level using molecular docking, MD simulation, and binding free energy calculations. The binding mode of BSA-drug3 is different from those of BSA-drug1 and BSA-drug2, which is mainly ascribed to their different chemical structures. The computed binding energies are consistent with available experimental results. The calculated free energies of BSA-drug1, BSA-drug2 and BSA-drug3 reveal that the binding site of drug1 is more stable than those of drug2 and drug3. The energy decomposition analysis shows that the electrostatic interactions play an important role in the stabilization of the binding site of BSA-drug1 while the van der Waal interactions contribute largely to stabilization of the binding sites of BSA-drug2 and BSA-drug3. The residue decomposition analysis illustrates that Lys138 is the key residue for binding sites of BSA-drug1 and BSA-drug2 while Leu421 and Tyr424 are two key residues for the binding site of BSA-drug3. The current MD simulation results provide insights into the mechanism of how drugs bind to BSA at the atomic level and will be useful for the development of an erythrocyte-based drug delivery system.

Acknowledgments The authors acknowledge the financial support by the research startup fund of Jilin University (No. 4305050102H8; No. 4305050102B5), the basic research and operational costs of Jilin University (No. 421031196604 and No. 450060445293), the Specialized Research Fund for the Doctoral Program of Higher Education (20090061120101), and the Natural Science Foundation of Jilin Province in China (20101552).

References

1. Haghi G, Hatami A (2010) Simultaneous quantification of flavonoids and phenolic acids in plant materials by a newly developed isocratic high-performance liquid chromatography approach. J Agric Food Chem 58:10812–10816
2. Rodrigues AS, Perez-Gregorio MR, Garcia-Falcon MS, Simal-Gandara J, Almeida DPF (2011) Effect of meteorological conditions on antioxidant flavonoids in Portuguese cultivars of white and red onions. Food Chem 124:303–308
3. Arct J, Pytkowska K (2008) Flavonoids as components of biologically active cosmeceuticals. Clin Dermatol 26:347–357
4. Kale A, Gawande S, Kotwal S (2008) Cancer phytotherapeutics: role for flavonoids at the cellular level. Phytother Res 22:567–577
5. Zhang S, Yang X, Coburn RA, Morris ME (2005) Structure activity relationships and quantitative structure activity relationships for the flavonoid-mediated inhibition of breast cancer resistance protein. Biochem Pharmacol 70:627–639
6. Kobori M, Masumoto S, Akimoto Y, Takahashi Y (2009) Dietary quercetin alleviates diabetic symptoms and reduces streptozotocin-induced disturbance of hepatic gene expression in mice. Mol Nutr Food Res 53:859–868
7. Salas MP, Celiz G, Geronazzo H, Daz M, Resnik SL (2011) Antifungal activity of natural and enzymatically-modified flavonoids isolated from citrus species. Food Chem 124:1411–1415
8. Huang XH, Xiong PC, Xiong CM, Cai YL, Wei AH, Wang JP, Liang XF, Ruan JL (2010) In vitro and in vivo antitumor activity of Macrothelypteris torresiana and its acute/subacute oral toxicity. Phytomedicine 17:930–934
9. Kim HJ, Lee SB, Park SK, Kim HM, Park YI, Dong MS (2005) Effects of hydroxy group numbers on the B-ring of 5,7-dihydroxyflavones on the differential inhibition of human CYP 1A and CYP1B1 enzymes. Arch Pharm Res 28:1114–1121
10. Tsujimoto M, Horie M, Honda H, Takara K, Nishiguchi K (2009) The structure-activity correlation on the inhibitory effects of flavonoids on cytochrome P450 3A activity. Biol Pharm Bull 32:671–676
11. Walle T (2007) Methoxylated flavones, a superior cancer chemopreventive flavonoid subclass? Semin Cancer Biol 17:354–362
12. Yang R, Zeng HJ, Yu LL, Chen XL, Qu LB, Li P (2010) The interaction of flavonoid-bsa and the relationship between molecular structure of flavonoids and their binding to BSA. Acta Chim Sin 68:1995–1999
13. Liu EH, Qi LW, Li P (2010) Structural relationship and binding mechanisms of five flavonoids with bovine serum albumin. Molecules 15:9092–9103
14. Huang BX, Kim HY, Dass C (2004) Probing three-dimensional structure of bovine serum albumin by chemical cross-linking and mass spectrometry. J Am Soc Mass Spectrom 15: 1237–1247
15. Peters T (1985) Serum albumin. Adv Protein Chem 37:161–245
16. He XM, Carter DC (1992) Atomic structure and chemistry of human serum albumin. Nature 358:209–215
17. Bolli A, Marino M, Rimbach G, Fanali G, Fasano M, Ascenzi P (2010) Flavonoid binding to human serum albumin. Biochem Biophys Res Commun 398:444–449
18. Matei L, Hillebrand M (2010) Interaction of kaemeferol with human serum albumin, a fluorescence and circular dichroism study. J Pharm Biomed Anal 51:768–773
19. Wackerbarth H, Stoll T, Gebken S, Pelters C, Bindrich U (2009) Carotenoidprotein interaction as an approach for the formulation of functional food emulsions. Food Res Int 42:1254–1258
20. Bi SY, Yan LL, Pang B, Wang Y (2012) Investigation of three flavonoids binding to bovine serum albumin using molecular fluorescence technique. J Lumin 132:132–140

21. Zhang YP, Shi SY, Sun XR, Xiong X, Peng MJ (2011) The effect of Cu^{2+} on interaction between flavonoids with different C-ring substituents and bovine serum albumin: structure-affinity relationship aspect. J Inorg Biochem 105:1529–1537
22. Shi XL, Li XW, Gui MY, Zhou HY, Yang RJ, Zhang HQ, Jin YR (2010) Studies on interaction between flavonoids and bovine serum albumin by spectral methods. J Lumin 130:637–644
23. Altschul SF, Madden TL, Schfer AA, Zhang JZ, Miller DJ (1997) Gapped BLAST and PSI-BLAST: a new generation of protein database search programs. Nucleic Acid Res 25:3389–3402
24. Wallner B, Elofsson A (2005) All are not equal: a benchmark of different homology modeling programs. Protein Sci 14:1315–1327
25. Montgomerie S, Cruz JA, Shrivastava S, Arndt D, Berjanskii M, Wishart DS (2008) PROTEUS2: a web server for comprehensive protein structure prediction and structure-based annotation. Nucleic Acid Res 36:202–209
26. Hess B, Kutzner C, Van der Spoel D, Lindahl E (2008) GROMACS 4: algorithms for highly efficient, load-balanced, and scalable molecular simulation. J Chem Theory Comput 4:435–447
27. Frisch MJ et al. (2009) Gaussian 09, Wallingford, CT, Gaussian 09 Revision A.02. Gaussian Inc, Wallingford
28. Morris GM, Huey R, Lindstrom W, Sanner MF, Belew RK, Goodsell DS, Olson AJ (2009) AutoDock4 and AutoDockTools4: automated docking with selective receptor flexibility. J Comput Chem 30:2785–2791
29. Hu R, Barbault F, Maurel F, Delamar M, Zhang R (2010) Molecular dynamics simulations of 2-amino-6-arylsulphonylbenzonitriles analogues as HIV inhibitors: interaction modes and binding free energies. Chem Biol Drug Des 76:518–526
30. Morris GM, Goodsell DS, Huey R, Olson AJ (1996) Distributed automated docking of flexible ligands to proteins: parallel applications of AutoDock 2.4. J Comput-Aided Mol Des 10:293–304
31. Hu R, Barbault F, Delamar M, Zhang R (2009) Receptor- and ligand-based 3D-QSAR study for a series of non-nucleoside HIV-1 reverse transcriptase inhibitors. Bioorg Med Chem 17:2400–2409
32. Jorgensen WL, Chandrasekhar J, Madura JD, Impey RW, Klein ML (1983) Comparison of simple potential functions for simulating liquid water. J Chem Phys 79:926–935
33. Ryckaert JP (1997) Numerical integration of cartesian equations of motion of a system with constrained molecular dynamics of N-alkanes. J Chem Phys 23:327–341
34. Berendsen HJC, Postma JPM, van Gunsteren WF, Dinola A, Haak JR (1984) Molecular dynamics with coupling to an external bath. J Chem Phys 81:3684–3690
35. Wang J, Wang W, Kollman PA, Case DA (2006) Automatic atom type and bond type perception in molecular mechanical calculations. J Mol Graph Model 2:247–260
36. Jakalian A, Jack DB, Bayly CI (2002) Fast, efficient generation of high-quality atomic charges. AM1-BCC model: II. Parameterization and validation. J Comput Chem 23:1623–1641
37. Vorontsov Ivan I, Miyashita Osamu (2010) Crystal molecular dynamics simulations to speed up MM/PB(GB)SA evaluation of binding free energies of di-mannose deoxy analogs with P51G-m4-cyanovirin-N. J Comput Chem doi:10.1002/jcc.21683
38. Jogalekar AS, Reiling S, Vaz RJ (2010) Identification of optimum computational protocols for modeling the aryl hydrocarbon receptor (AHR) and its interaction with ligands. Bioorg Med Chem Lett 20:6616–6619
39. Swanson JMJ, Henchman RH, McCammon JA (2004) Revisiting free energy calculations: a theoretical connection to MM/PBSA and direct calculation of the association free energy. Biophys J 86:67–74
40. Thanyada R, Nadtanet N, Maturos M, Nopporn K, Pathumwadee Y, Arthitaya M, Supot H (2010) Molecular insight into the specific binding of ADP-ribose to the nsP3 macro domains of chikungunya and venezuelan equine encephalitis viruses: Molecular dynamics simulations and free energy calculations J Mol Graph Model Published online
41. Han WW, Wang Y, Luo Q, Feng Y, Niu XD (2011) Insights into a 3D homology Model of arylesterase: the key residues upon protein-ligand docking and mm_pbsa calculations. J Theor Comput Chem 10:165–177
42. Baker NA, Sept D, Joseph S, Holst MJ, McCammon JA (2001) Electrostatics of nanosystems: application to microtubules and the ribosome. Proc Natl Acad Sci U S A 98:10037–10041
43. Punkvang A, Saparpakorn P, Hannongbua S, Wolschann P, Beyer A, Pungpo P (2010) Investigating the structural basis of arylamides to improve potency against M. tuberculosis strain through molecular dynamics simulations. Eur J Med Chem 45:5585–5593
44. Schaffner-Barbero C, Gil-Redondo R, Ruiz-Avila LB, Huecas S, Lappchen T, den Blaauwen T, Diaz JF, Morreale A, Andreu JM (2010) Insights into nucleotide recognition by cell division protein FtsZ from a mant-GTP competition assay and molecular dynamics. Biochemistry 49:10458–10472